energies

MDPI

Article

Integration of Floating Photovoltaic Panels with an Italian Hydroelectric Power Plant

Paolo Venturini, Gabriele Guglielmo Gagliardi *, Giuliano Agati, Luca Cedola, Michele Vincenzo Migliarese Caputi and Domenico Borello

Department of Mechanical and Aerospace Engineering, Sapienza University of Rome, 00184 Rome, Italy; paolo.venturini@uniroma1.it (P.V.); giuliano.agati@uniroma1.it (G.A.); luca.cedola@uniroma1.it (L.C.); michelevincenzo.migliaresecaputi@uniroma1.it (M.V.M.C.); domenico.borello@uniroma1.it (D.B.)
* Correspondence: gabriele.gagliardi@uniroma1.it

Abstract: The potential of applying a floating PV (FPV) system in an Italian context (namely, Cecita dam and Mucone hydroelectric power plants) is studied. The additional PV energy production, as well as the effect of non-evaporated water on the productivity of the hydropower plant, is analyzed by varying the basin surface coverage. The simulations highlight that the amount of additional hydroelectricity is quite small if compared to the non-FPV system, reaching about 3.56% for 25% basin surface coverage. However, the annual PV energy production is noticeable even at low coverage values. The expected gain in electricity production in the case of 25% basin surface coverage with the FPV plant rises to 391% of that of the actual hydropower plant. This gain becomes even larger if a vertical axis tracking system is installed and the increase is about 436%. The economic analysis confirms that the production costs (USD/kWh) of FPV systems are comparable to those of land-based PV (LBPV) plants, becoming smaller in the case that a tracking system is installed. In particular, the best solution is the one with 15% coverage of the lake. In this case, the levelized cost of electricity for the LBPVs is 0.030 USD/kWh and for the FVPs, with and without tracking, it is equal to 0.032 and 0.029 USD/kWh, respectively.

Keywords: floating PV; hydro/PV coordinated operation; hydroelectric power plant; numerical modeling; solar energy

Citation: Venturini, P.; Gagliardi, G.G.; Agati, G.; Cedola, L.; Migliarese Caputi, M.V.; Borello, D. Integration of Floating Photovoltaic Panels with an Italian Hydroelectric Power Plant. *Energies* **2024**, *17*, 851. https://doi.org/10.3390/en17040851

Academic Editors: Francesco Calise, Qiuwang Wang, Poul Alberg Østergaard, Maria da Graça Carvalho, Wenxiao Chu and Maria Vicidomini

Received: 12 December 2023
Revised: 29 January 2024
Accepted: 31 January 2024
Published: 11 February 2024

1. Introduction

Aiming at achieving climate neutrality by 2050, in July 2021, the European Commission adopted the 'Fit for 55' package [1] to reach a 55% reduction in greenhouse gas emissions by 2030 compared to 1990's levels. Each of the member states, according to its abilities and its technology, is committed to supporting such an ambitious aim. In this context, Italy's growth appears too slow to be in line with the new EU 2030 targets, despite 2020 targets having been reached and exceeded (20% renewable energy sources vs. 17% as the target [2]). In fact, in the Integrated National Energy and Climate Plan [3], it was estimated that, for Italy, the percentage of energy consumption from renewable sources (30%) was lower than the 32% required by the European Union. Therefore, the application of the national plan mentioned above requires a rapid improvement in the share of renewable energy to reach the 'Fit for 55' targets with the double aim of enhancing the production of sustainable energy used while reducing environmental pollution [4]. It has been estimated that this will require a share of renewable electricity of about 72% in 2030 [5], which is far from about 40% in 2020.

In 2021, the renewable energy source that most contributed to electricity generation in Italy was hydropower (about 39.0% of the total), followed by solar (about 21.5%) and wind energy (about 18.0%) [6]. Historical trends of installed power (Figure 1a) and energy production (Figure 1b) show how hydropower almost reached its maximum capacity, with

strong oscillations in energy production due to the annual variations in weather conditions. On the other hand, wind and PVs are growing with a trend related to installation costs, smaller infrastructure, and policy initiatives.

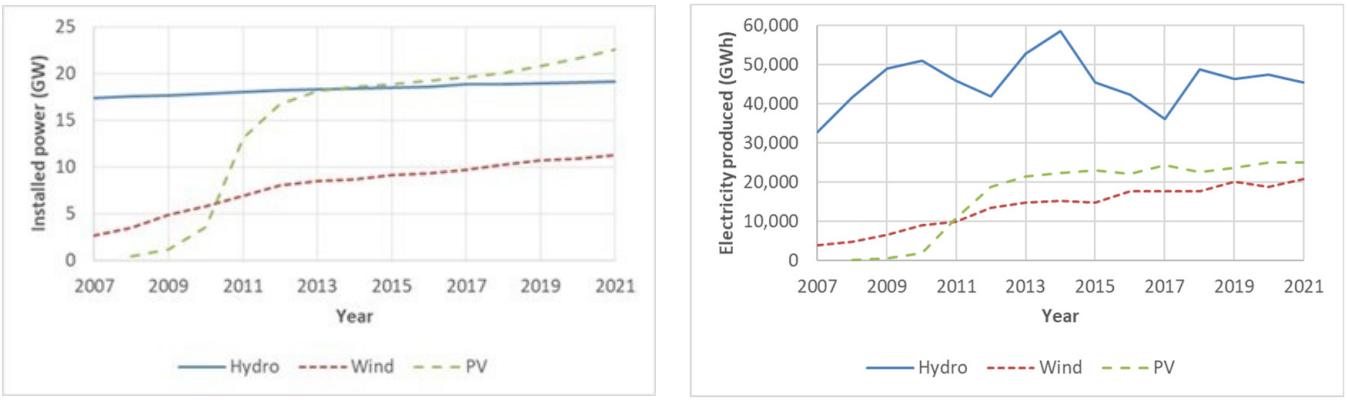

(**a**) (**b**)

Figure 1. Hydro, wind, and PVs in Italy: installed power (**a**) and energy production (**b**) (data: [4]).

To reach the EU targets for emission reduction, Italy should install 60–70 GW of wind and solar power systems by 2030 [7]. The main limiting factor for the widespread implementation of PV systems on a large scale lies in land use. The limited efficiency of PV modules, typically around 20%, results in a significant land requirement (i.e., for the installation of a 1 MWp power station, at least 10,000 m^2 of land is needed). In Italy, cities often have large historical centers that cannot be used (or hardly used) for PV applications, thus forcing operators to consider ground-based PV applications as the only way to increase renewable energy shares. This land usage has a notable environmental impact, as it makes the land unsuitable for alternative uses, namely food production. Despite a slight mitigation of the issue through a rise in the PV module efficiency to 21%, related to the nature of the semiconductors that are commonly used in this kind of application [8,9], the problem of land usage remains, thus slowing down the growth of the PV market, as occurred in past years [10]. Taking as reference the solutions already adopted for wind farms, the deployment of floating PV (FPV) power plants appears to be a suitable solution for sustaining a more pronounced growth of PV-based electricity production. The cost of FPVs is comparable to that of land-based PVs (LBPVs), and the potential of using vast water surfaces is highly significant. The main advantages of FPVs against LBPVs are reported here [11].

1. Strong reduction in land occupancy: FPVs provide a way to keep land for other uses, thus avoiding competition with agricultural and green areas (risk of indirect land use change.
2. Limiting albedo effect: The albedo effect on land typically ranges from 20 to 30%, whereas the reflection from PV modules does not exceed 5% and that from water is about 5–6%. Therefore, the installation of FPV plants does not alter the radiation balance, as is the case with LBPV systems.
3. Water savings: Since the use of FPVs results in partial coverage of the selected water surface (by the PV module and floating structures), a reduction in water evaporation is expected, thus increasing the water reserve for hydropower production or other uses.
4. Cooling and tracking: The installation of PV modules on a water basin leads to an easier cooling of the modules due to humidity, which, in turn, results in an increase in module efficiency compared to land installations. Moreover, FPVs allow the installation of simple vertical axis tracking systems [12], providing a gain in yearly produced energy up to 25% [12].

On the other hand, there are two main disadvantages associated with the use of FPV systems [13]:

1. Technical: Possible breakage of the photovoltaic modules due to harsh atmospheric conditions, fast degradation of the materials due to the (possible) salinity of water, difficult maintenance operations.
2. Environmental: Possible impact on the natural environment and the biodiversity present in the water body.

In fact, it is well known that covering the water surface of an existing reservoir irreparably changes its environment. Without sunlight beneath the water's surface, biological life would suffer, and in extreme situations, it may go extinct. Furthermore, the materials used in PV panels have well-known hazardous effects on the environment [14]. All these aspects have been investigated by Rosa-Clot [14]. For long-term operation, the cleaning of FPV systems is easier than that of LBPV systems, so less water and chemicals are needed, which ultimately reduces water pollution. In addition, the FPV systems do not seem to significantly affect birdlife. Furthermore, Cazzaniga et al. [15] noted the advantage of partially covering water bodies that are affected by rapid algal growth due to eutrophication.

The first small-scale (about 20 kWp) FPV system was installed in Aichi (Japan) in 2007, followed by several other small projects in France, Italy, South Korea, Spain, and the USA. All of these projects were developed for research or demonstration purposes. In California, the first commercial application of FPVs (175 kWp) was installed at the Far Niente Winery in 2008. The first FPV application larger than 1 MWp dates back to 2013 [16]. Although the number of installations is still small, FPVs are growing rapidly. With 339 projects active in more than 35 countries, the installed capacity of FPVs was around 2.6 GWp in 2020. Growth has increased in the last three years, with about 3.8 GWp installed, reaching a cumulative capacity of around 5.7 GWp in 2022 (Figure 2). The largest installed plant (150 MWp) is in China, but several large projects are being planned and realized in other countries. Future demand for FPVs is expected to be driven by Asian countries [17], but there is also room for improvement in the EU, including Italy.

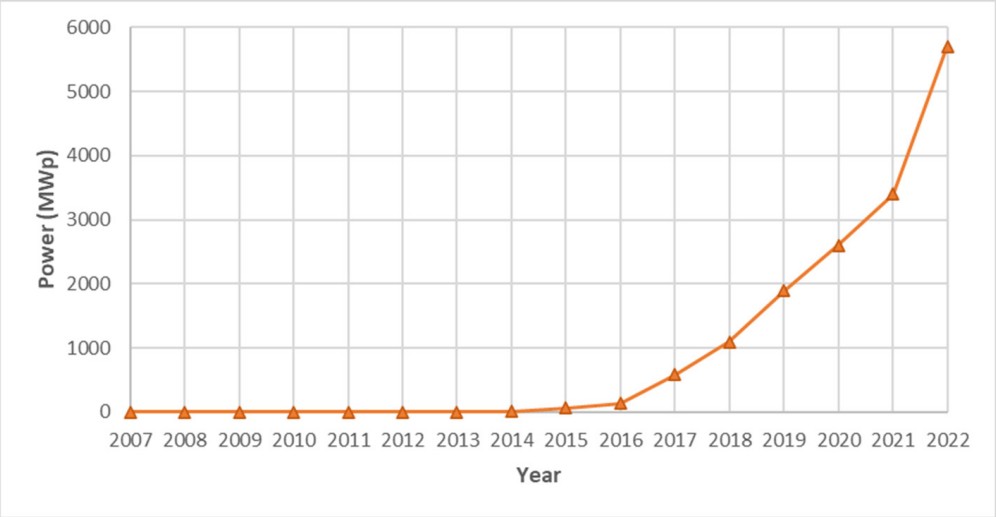

Figure 2. Global installed FPV capacity between 2007 and 2022 (data source: [16,18]).

The objective of this paper is to assess the potential of an FPV system coupled to a hydropower plant fed by the Cecita dam, located in southern Italy where water basins are strongly affected by evaporation because of the higher temperatures and solar radiation. Table 1 summarizes the annual average daily temperature and solar radiation in three Italian cities: Bolzano in the north, representing the region where most of the Italian hydropower plants are located, Rome in the center, and Catanzaro in Calabria, where Lake Cecita is located. As expected, the average temperature and irradiance increase as one moves

south in Italy. Polemio and Casarino [19] demonstrated that southern Italy (especially Calabria) is affected by cyclical drought periods, affecting flora and water reservoirs [20]. Spinoni et al. [21] found that droughts will increase in the Mediterranean area during the XXI century due to the increase in greenhouse gas emissions, with southern Italy being one of the most exposed regions.

Table 1. Annual average daily temperature and irradiance in the Italian cities of Bolzano, Rome, and Catanzaro (data source: PVGIS online tool).

City	Annual Average Daily Temperature (°C)	Annual Average Daily Irradiance on the Horizontal Plane (W/m^2)
Bolzano	8.02	165.97
Rome	15.82	159.87
Catanzaro	16.12	184.81

The productivity of the hybrid plant considered here was estimated under different configurations. An economic analysis is also performed to compare the levelized cost of electricity (LCOE) of an FPV system against that of an LBPV system.

Floating Photovoltaic Systems

A sketch of an FPV system is reported in Figure 3. It consists of the following main components:

1. Floats (which can be made of different materials and shapes) to support the PV modules and provide a safe support and walking surface for the operators;
2. PV modules (the same as in the LBPV plants, but with a different solar tracking system);
3. Mooring and anchoring system (the configuration depends on the water profile and soil conditions in the basin) to reduce lateral movement and unwanted rotation, as well as the risk of collision with nearby shorelines or other floating objects;
4. Electrical components: electrical cables, inverters, transformers, etc., as in an LBPV system.

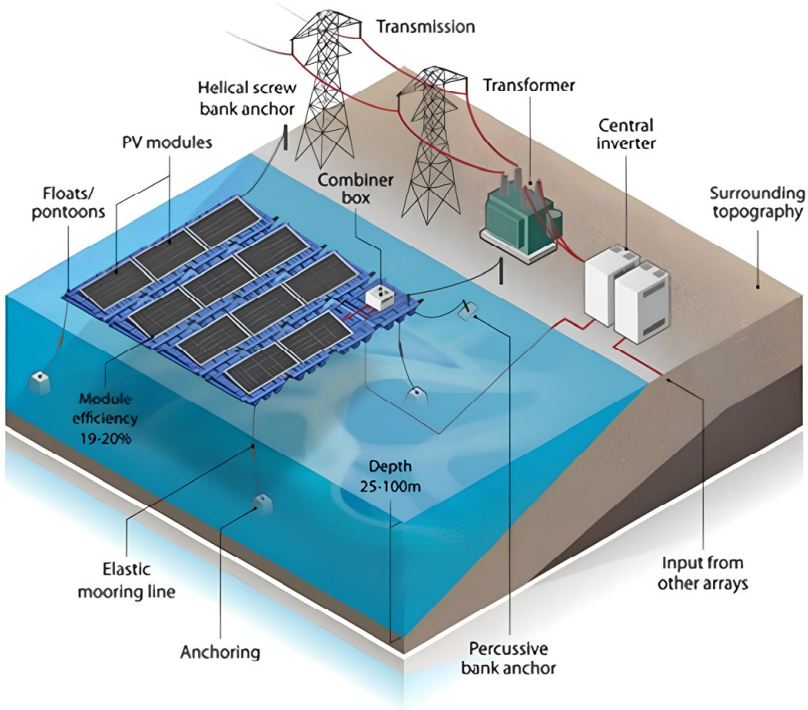

Figure 3. Sketch of an FPV system [22] (image credit: Alfred Hicks, NREL).

A significant factor to consider in FPV systems is the tilt angle of the modules. In LBPV applications, it is set to maximize energy production. In the case of FPVs, the tilt angle is smaller than that of LBPV systems to mitigate the effects of the wind on the system, which can cause movement of the photovoltaic field, overturning, breaking of anchors/moorings, damage to support structures and modules, etc. [16,22–24]. Trapani and Santafé [25] analyzed various FPVs installed in the period 2007–2013 and reported that in Italy and Spain the tilt angle is usually limited to about 10°. In [16,26], the authors report that in FPV installations the maximum tilt angle is 10–15° to minimize drag and lift forces. On the other hand, a reduced tilt angle results in a limited shading effect, which in turn leads to a smaller distance between two strings of PV modules, thus reducing the occupancy of the water surface [25].

2. Mathematical Modeling

The applied models for the evaluation of the potential of an FPV system in terms of avoided water evaporation and electricity production are described below.

2.1. Estimating Open Water Evaporation

Water evaporation is affected by two main factors: meteorological conditions and properties of the water body. In terms of meteorological conditions, the net radiation is the key parameter as it is closely correlated with the energy captured by the water and thus the evaporation rate. Wind speed and humidity influence the diffusion process of water molecules from the body to the air. Some of the properties of water bodies depend on water depth, surface area (which affects the thermal stratification), and salinity. Others are related to external conditions, such as rainfall and vegetation [27]. Developing a prediction model that takes all these factors into account is quite complex and requires many parameters to be calibrated, making it difficult to develop reliable prediction methods [9].

There are several models available in the literature to estimate the evaporation rate of a water body. Finch and Hall [28] classified all these models into seven categories: pan evaporation, mass balance, energy budget, bulk transfer, combination, equilibrium temperature, and empirical factors. Pan evaporation, dating back to the 18th century, uses water pans to measure evaporation. However, it is not accurate in real field applications. Mass balance models estimate the evaporation rate (ER) as the change in water storage volume and the difference between inflow and outflow. For practical applications, the energy budget models estimate ER as the contribution needed to close the energy budget, while the bulk transfer models estimate ER based on the difference between saturated and reference air vapor pressure. In 1948, Penman [29] developed a model that combined mass transfer and energy budget approaches, eliminating the need for water surface temperature. Nowadays, the Penman and Penman–Monteith models are widely used for estimating open water evaporation due to their accuracy. They have become a reference for the Food and Agriculture Organization of the United Nations [30], the American Society of Civil Engineers [31], and several scientists worldwide. Researchers introduced a method for estimating water temperature in equilibrium temperature models. Empirical factors have been used to convert evaporation measurements for different land surfaces.

All the previous models require knowing or computing several quantities or correction factors, which are not always readily available in the literature or from meteorological data. Therefore, estimating ER is extremely complex. Bontempo Scavo et al. [32] recently assessed several evaporation models and derived a simplified approach based on experiments, accounting for some of the most relevant quantities affecting the evaporation rate. The authors compared the predictions of six different evaporation models with real field evaporation data. They found that the Penman–Monteith model was the most accurate, then developed and evaluated two linear regression models and three Design of Experiment (DoE) models based on the Penman–Monteith model.

In the present work, the linear regression model is used, Equation (1) [32], which uses four meteorological quantities to estimate the ER. In Equation (1), R_S is the daily

horizontal solar radiation (MJ/m^{2}d); T is the main daily temperature (°C); RH is relative humidity (%); u_{10} is the daily wind speed at 10 m above sea level (m/s). This model strikes a good balance between accuracy and complexity. Indeed, the four meteorological quantities required can be easily obtained or computed using the PVGIS (Photovoltaic Geographical Information System) online tool [33]. According to [32], the percentage error between reference measurements and the linear model considered for open water evaporation is approximately 2.0%, indicating a very good agreement and accuracy. Table 2 provides a summary of the comparison between reference measurements and some of the models reported in [32].

Table 2. Comparison of cumulated evaporation and model prediction (data source: [32]).

	Measures	**PM [34]**	**V [35]**	**R [36]**	**LR4 [32]**
Cumulated evaporation (mm)	303.21	309.82	293.99	268.49	297.05
Deviation from measurements (%)	0.00	−2.18	3.04	11.45	2.03

PM: Penman–Monteith [34]; V: Valiantzas [35]; R: Rohwer [36]; LR4: linear regression (4 variables) [32].

When an FPV system is installed, the ER is reduced because the water surface is partially covered by PV panels and/or floats [32]. If an FPV system is used in which floats completely cover the surface below the module (as shown in Figure 2), the evaporation rate can be calculated using Equation (2) [32], where x represents the coverage ratio (fraction of the water surface covered by FPVs).

$$ER_{free} = 2.421 + 0.012 \cdot R_S + 0.159 \cdot T - 0.056 \cdot RH + 0.122 \cdot u_{10} \quad (1)$$

$$ER_{PVcover} = 2.421 + (1 - x)0.012 \cdot R_S + 0.159 \cdot T - 0.056 \cdot RH + 0.122 \cdot u_{10} \quad (2)$$

2.2. Estimating the Gain in Hydropower Production

The annual evaporated water in the cases of free (AEW_{free} Equation (3)) and covered ($AEW_{PVcover}$, Equation (4)) basins can be estimated by multiplying the water surface S_w by ER (Equations (1) and (2)) and summing the results for the 365 days in a year. Equation (5) gives the evaporated water in the case of a surface partly covered by FPVs (AEW_{FPV}).

$$AEW_{free} = \sum_{day=1}^{365} E_{free,day} S_W \quad (3)$$

$$AEW_{PVcover} = \sum_{day=1}^{365} E_{PVcover,day} x S_W \quad (4)$$

$$AEW_{FPV} = AEW_{free} \cdot (1 - x) + AEW_{PVcover} \cdot x \quad (5)$$

In Equations (3) and (4), it is assumed that S_W is independent of the water level in the basin. The difference $AEW_{saved} = AEW_{free} - AEW_{FPV}$ represents the annual amount of water saved due to the presence of the FPV system. This water is available for hydropower production, resulting in a net gain for the hydroelectric plant.

The energy surplus, E_{gain}, produced by the hydropower plant due to AEW_{saved} is computed assuming a global efficiency $\eta_g = 75$ % for the plant [37]. Therefore, it is possible to write

$$E_{gain} = \eta_g g \varrho h \dot{V} t \quad (6)$$

where g = 9.81 m/s^2 is the gravity acceleration, ρ the water density, h the water head, $\dot{V}$ the volumetric flow rate of water, and t the time needed to consume AEW_{saved} assuming a constant volumetric flow rate ($\dot{V}$).

2.3. Estimating FPV Productivity

To estimate the productivity of the FPV system, the irradiation data provided by PVGIS [15] are taken as reference. After determining the module type, the installed peak power, tilt and azimuth angles, and BOS (Balance Of System) losses of the system, PVGIS provides (among other information) the average monthly energy production of the given system (in kWh/month). However, this estimation is based solely on the module efficiency as determined by the PVGIS tool and does not account for the cooling effect of water. Indeed, this aspect should be considered in a successive analysis. The annual energy production is estimated according to Equation (7), which takes into account the average monthly sum of global irradiation per square meter ($H_{mo,i}$) received by the modules (in kWh/m^{2}mo).

$$E = \sum_{i=1}^{12} H_{mo,i}\, S_{PV} \eta_{PV} \eta_{cool} \eta_{BOS} \quad (7)$$

$$S_{PV} = x S_W / cos\alpha \quad (8)$$

where S_{PV} is the total surface of the FPV system, computed by fixing a coverage fraction and the tilt angle α (Equation (8)); η_{PV} is the module efficiency; η_{cool} (>1.0) is the efficiency gain due to the cooling effect of the water basin; and η_{BOS} is the efficiency of the BOS.

2.4. The Cecita Dam Hydroelectric Power Plant

Lake Cecita is an artificial reservoir located in the heart of the Sila Grande (Sila Plateau, Calabria, Italy, Figure 4). It covers an area of about 12.6 km^2 and was created by damming the Mucone river. The arch-gravity dam (Figure 5) was built between 1955 and 1956 and forms the largest reservoir in Calabria. It is primarily used for hydroelectric power generation.

Figure 4. Lake Cecita and dam (red line) location (© OpenStreetMap, https://www.openstreetmap.org/copyright).

Figure 5. Cecita dam (source: https://www.enelgreenpower.com/; accessed on 20 January 2024).

The Cecita dam is 50 m high, with the crest at 1145 m above sea level and a total reservoir capacity of about 108 Mm^3 [38,39]. The hydroelectric power plant is divided into two plants (namely Mucone I and Mucone II), each exploiting two different water jumps. The Mucone I plant is located in Acri (Cosenza, Italy), about 14 km from the Cecita dam and exploits a 629.5 m water jump. It is composed of two Pelton turbines, 55 MW each, and 20 m^3/s is the maximum water flow rate. The efficient power is 100 MW and the average annual energy production equals 175.0 GWh. The Mucone II plant is located close to Luzzi (Cosenza, Italy) about 10 km downstream from Mucone I. It exploits a 306.1 m water jump, and it is composed of two Francis turbines, 27 MW each, with a total efficient power of 50 MW and 20 m^3/s as the maximum water flow rate [38,40]. Table 3 summarizes the main characteristics of the two hydroelectric power plants.

Table 3. Main characteristics of Mucone I and Mucone II hydroelectric plants.

Mucone I Power Plant	Mucone II Power Plant
Geodetic jump 641 m	Geodetic jump 308.75 m
Average useful jump 629.50 m	Average useful jump 306.10 m
Maximum derivable flow rate 20.00 m^3/s	Maximum derivable flow rate 20.00 m^3/s
Turbine type: Pelton	Turbine type: Francis
Installed power 112,440 kW	Installed power 55,000 kW
Efficient power 100,000 kW	Efficient power 50,000 kW
Average annual producible energy 175 GWh	Average annual producible energy 110 GWh
Forced diversion tunnel: length 13,618 m, circular cross-section, diameter 2.95 ÷ 2.70 m	Forced diversion tunnel: length 9755 m, circular cross-section, diameter 3.30 m
Vertical piezometric well: height 111 m, diameter 6.50 ÷ 10.80 m	Vertical piezometric well: height 36 m, diameter 12.80 ÷ 20.00 m
Inclined piezometric pipe: length 200 m, diameter 1.50 m, inclination 83%	Vertical piezometric pipe: height 46 m, diameter 2.80 m
Penstock: length 843.50 m, diameter 2.50 ÷ 2.00 m	Penstock: length 1150.50 m, diameter 2.95 ÷ 2.30 m

2.5. FPV Energy Production

Two possible configurations of the FPV system have been considered. In a configuration named FPV_noTrack, the PV modules are assumed to be placed at a 0° azimuth angle and 15° tilt angle (to avoid issues in the case of high-speed winds). In the second configuration (FPV_Track), a vertical axis tracking system is added to carry out useful comparisons with FPV_noTrack.

3. Results

A series of simulations were conducted to predict the annual evaporation of the Cecita basin with a coverage fraction x ranging from 5 to 25%. The evaporation rate is computed with and without the presence of an FPV system according to Equations (1) and (2), respectively. In Figure 6, the daily evaporation rates with an FPV system (x = 0.25; orange dashed line) or in open water (blue continuous line) are reported. As expected, the maximum evaporation rate, in both cases, is predicted during summertime, and the minimum during wintertime, primarily due to the difference in average temperature. The trends of cumulative evaporation rate are shown in Figure 7.

The cumulative difference between the two extreme cases is about 420 mm/y, which is a significant value considering the surface area of the basin. In fact, this difference corresponds to about 5.31 Mm^3/y (the total volume of the basin is about 108 Mm^3). Table 4 summarizes the quantity of non-evaporated water (NEW) for all the considered x values and the time required to consume it (at maximum flow rate) as a function of x.

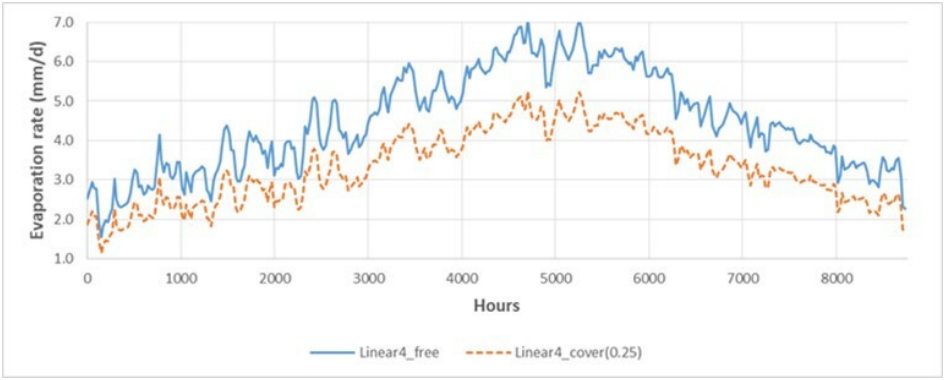

Figure 6. Daily evaporation rate of open (blue continuous line) and covered (orange dashed line) water (x = 0.25).

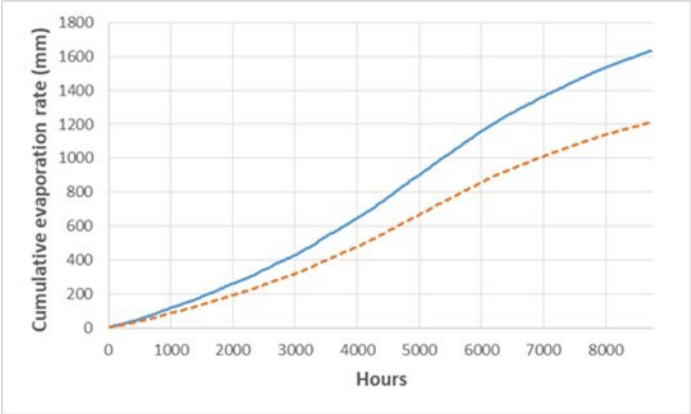

Figure 7. Cumulative evaporation rate of open (blue line) and covered (orange line) water (x = 0.25).

Table 4. Non-evaporated water and time to consume it at maximum flow rate, as a function of the coverage ratio (NEW: non-evaporated water; NEWV: non-evaporated water volume).

x	x = 0.00 (Free)	x = 0.05	x = 0.10	x = 0.15	x = 0.20	x = 0.25
ER (mm/y)	1633.3	1548.3	1463.7	1379.4	1295.5	1211.9
NEW (mm/y)	0.0	85.0	169.6	253.9	337.9	421.4
NEWV (m^3/y)	0	1,070,851	2,137,296	3,199,334	4,256,967	5,310,193
Time to consume NEWV at max flow rate (h)	0.0	14.9	29.7	44.4	59.1	73.8

For the largest x value considered (i.e., 0.25), the volume of non-evaporated water equals 5.31 Mm^3/y, which corresponds to about 74 h of additional power production in maximum flow rate conditions. This value increases the energy potential of the basin. For x = 0.05, an additional 1.08 Mm^3/y of non-evaporated water is available, corresponding to about 15 h of new power production. The recoverable energy is reported in Table 5: for x = 0.25, the additional electricity production is 10.154 GWh, which is about 3.56% more than the case without FPVs. For x = 0.05, it is only about 1.0%.

Table 5. Additional electricity producible by the non-evaporated water.

Recoverable Energy (kWh)	x = 0.00 (Free)	x = 0.05	x = 0.10	x = 0.15	x = 0.20	x = 0.25
Jump I	0	1,377,693	2,749,718	4,116,074	5,476,760	6,831,779
Jump II	0	669,916	1,337,075	2,001,478	2,663,124	3,322,013
Total	0	2,047,609	4,086,793	6,117,551	8,139,884	10,153,792
% with regard to x = 0.0	0.00%	0.7%	1.4%	2.1%	2.9%	3.6%

The simulation results are consistent with the literature. Abdelgaied et al. [41] investigated the possibility of covering Lake Nasser (Egypt) with floating panels for both environmental and energy purposes. They used the Penman–Monteith method to estimate water evaporation and observed that increasing the covered area of the lake resulted in greater water evaporation savings. Since the weather conditions are different in terms of temperature and relative humidity (Egypt is in a hotter climate range than Italy), by assuming a fixed coverage ratio of 20% they estimated a higher water saving percentage: 30% against 21% calculated in this study.

The average monthly global irradiations per unit of surface received by the PV modules, with and without the VA tracking system, are reported in Figure 8. The benefits of using a VA tracking system are demonstrated in Figure 9. The largest gain (about 17%) is observed during the summer months of June and July, with a decrease to 4% in January and December. The annual average gain is about 10%.

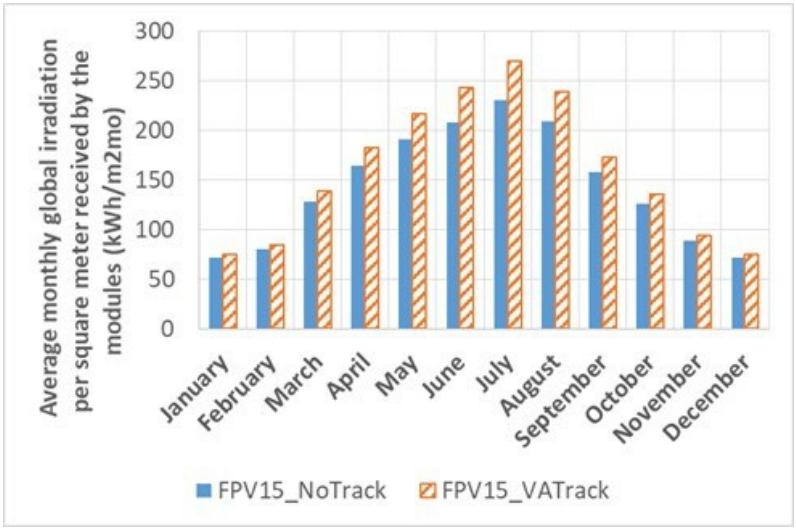

Figure 8. Average monthly global irradiation per m^2 received by the modules of the given system with and without a vertical axis (VA) tracking system.

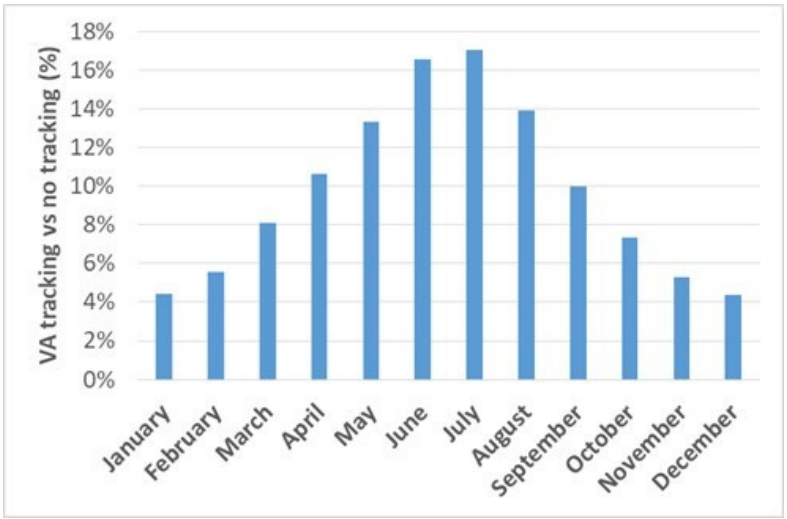

Figure 9. Gain (%) of average monthly global irradiation per m^2 received by the modules with VA tracking system compared to without VA tracking system.

In the present simulations, a 500 Wp monocrystalline silicon PV module is considered as a reference, and the main characteristics are summarized in Table 6 [42]. The BOS efficiency is assumed equal to 86%. In warm regions with a global horizontal irradiation exceeding approximately 1600 kWh/m^{2}y, FPV systems are expected to perform 10% better than LBPV systems [16,43,44]. The nominal irradiation is 1558 kWh/m^{2}y, and a 9% gain due to cooling effect (i.e., η_{cool} = 1.09) is assumed.

Table 6. Main characteristics of the reference PV module [42].

Characteristic	Value
Peak power (Wp)	500 W
Voltage at Wp (Vmp)	38.3 V
Current at Wp (Imp)	13.05 A
Open circuit voltage (Voc)	45.7 V
Short circuit current (Isc)	13.92 A
Module efficiency	21.10%
Weight	25.5 Kg
Size	2094 × 1134 × 35 mm
Surface	2.375 m^2

The peak power of the FPV system (Table 7) is related to the coverage ratio, which ranges from 5 (137 MWp) to 25% (637 MWp). When assuming a 5% coverage, the peak power of the FPV system is of the same order of magnitude (92%) as that of the hydropower plant. The system in this case is composed of 274,667 PV modules and covers approximately 0.652 km^2 of net surface. According to Cazzaniga et al. [43], the FPV plant should have a nominal power close to that of the hydroelectric power plant to reduce the hydro turbines' energy production during the sunny hours without reducing the electricity sent to the grid, as in the case of 5% coverage. When the surface coverage is 25%, the power of the FPV system is more than four times greater than that of the hydropower plant. The system in this configuration is composed of 1,373,336 PV modules occupying a net area of 3.26 km^2.

Table 7. FPV system characteristics.

x	0.05	0.10	0.15	0.20	0.25
# of FPV modules	274,667	549,334	824,002	1,098,669	1,373,336
FPV net surface (m^2)	652,223	1,304,446	1,956,672	2,608,895	3,261,118
FPV plant Wp (MW)	137.3	274.7	412.0	549.3	686.7
% with regard to hydropower	92%	183%	275%	366%	458%

Table 8 presents a comparison of the annual electricity production in the two considered floating configurations. The FPV_Track system generates more energy for all x values. Despite having only a 5% coverage ratio, the annual energy production of the FPV system is comparable to that of the hydroelectric plant, reaching 248.401 GWh/y, which is about 87% (in FPV_Track configuration) that of the hydroelectric production. When x = 0.25, the annual energy production is 391% and 436% (without and with VA tracking system, respectively) that of the hydroelectric plant, confirming the great potential of this solution.

Table 8. Annual energy production of the FPV systems as a function of x.

			x		
Configuration	0.05	0.1	0.15	0.2	0.25
FPV_noTrack (GWh/y)	223.022	446.045	669.068	892.090	1115.113
% with regard to hydropower	78%	157%	235%	313%	391%
FPV_Track (GWh/y)	248.401	496.803	745.205	993.606	1242.008
% with regard to hydropower	87%	174%	261%	349%	436%

An economic analysis is also carried out to compare the production cost of electricity produced through an FPV system with an LBPV system. Since FPVs are not as widespread as LBPVs, the costs are estimated. The capital expenditure (CAPEX) of an FPV system is higher than that of an LBPV system due to the floats, mooring and anchoring systems, etc., but the gap varies significantly. According to [7], the CAPEX cost for FPVs is 730 USD/kWp for a 50 MWp FPV plant, which is consistent with the estimates of Goswami et al. [45], who indicate a CAPEX cost of FPVs equal to 940 USD/kWp for a 10 MWp FPV system in India. Rosa-Clot et al. [46] assumed a CAPEX of 1100 USD/kWp for a techno-economic analysis of an FPV system in Australia. An NREL study [9] indicates a CAPEX of 1050 USD/kWp for a 50 MWp system, increasing to 1680 USD/kWp for 2.0 MW FPV plants in the USA.

For the present study, the costs indicated in [16] and summarized in Table 9 are adopted. Additionally, the costs of inverter replacement after 10 years and decommissioning of the system at the end of the plant lifetime (20 years) were included in the analysis, assuming a fixed rate of 10% of the total CAPEX. A constant 4% actualization rate is assumed, and neither loan nor plant insurance were considered. Operational expenditure (OPEX) is assumed to be 2.5% of total CAPEX.

Table 9. FPV vs. LBPV: CAPEX and OPEX.

	FPV	**LBPV**
PV modules (USD/Wp)	0.25	0.25
Inverters (USD/Wp)	0.06	0.06
Mounting system (USD/Wp)	0.15	0.10
BOS (USD/Wp)	0.13	0.08
Design, construction, T&C (USD/Wp)	0.14	0.13
Total CAPEX (USD/Wp)	0.73	0.62
Plant decommissioning (10% of total CAPEX; USD/Wp)	0.073	0.062
OPEX (2.5% of total CAPEX; USD/Wp/y)	0.01825	0.0155

The cost of the tracking systems is estimated based on Farrar et al. [24]. Consequently, a 20% larger CAPEX for the FPV system with a VA tracking system compared to a fixed FPV system is assumed (Table 9).

The production cost of FPV_noTrack and FPV_Track configurations is compared to that of an LBPV system of the same size but without a sun tracking system. Optimal tilt angle (31°) is considered in the LBPV plant, while tilt angle is fixed at 15° in FPVs. The actualized costs (CAPEX, OPEX, device replacements, and plant decommissioning) of the three configurations considered, as a function of the surface coverage ratio, are reported in Tables 10–12.

Table 10. FPV_noTrack actualized costs.

	x = 0.05	x = 0.10	x = 0.15	x = 0.20	x = 0.25
Total CAPEX (USD)	100,253,455	200,506,910	300,760,730	401,014,185	501,267,640
OPEX (2.5%/y CAPEX; USD)	2,506,337	5,012,673	7,519,018	10,025,355	12,531,691
Actualized OPEX (20 y; USD)	34,061,929	68,123,859	102,185,912	136,247,841	170,309,770
Inverter replacement (after 10 y; USD)	5,566,655	11,133,311	16,699,986	22,266,642	27,833,297
Plant decommissioning (USD)	4,575,437	9,150,8743	13,726,327	18,301,764	22,877,201
Total actualized costs (USD)	144,457,477	288,914,953	433,372,956	577,830,432	722,287,909

Table 11. FPV_Track actualized costs.

	x = 0.05	x = 0.10	x = 0.15	x = 0.20	x = 0.25
Total CAPEX (USD)	102,176,124	204,352,248	306,528,744	408,704,868	510,880,992
OPEX (2.5%/y CAPEX; USD)	2,554,403	5,108,806	7,663,219	102,17,622	12,772,025
Actualized OPEX (20 y; USD)	34,715,172	69,430,343	104,145,642	138,860,813	173,575,985
Inverter replacement (after 10 y; USD)	5,566,656	11,133,311	16,699,987	22,266,642	27,833,298
Plant decommissioning (USD)	4,663,185	9,326,370	13,989,572	18,652,757	23,315,942
Total actualized costs (USD)	147,121,136	294,242,272	441,363,944	588,485,080	735,606,216

Table 12. LBPV (fixed optimal tilt) actualized costs.

	x = 0.05	x = 0.10	x = 0.15	x = 0.20	x = 0.25
Total CAPEX (USD)	85,146,770	170,293,540	255,440,620	340,587,390	425,734,160
OPEX (2.5%/y CAPEX; USD)	2,128,669	4,257,338	6,386,015	8,514,684	10,643,354
Actualized OPEX (20 y; USD)	28,929,309	57,858,619	86,788,034	115,717,344	144,646,654
Inverter replacement (after 10 y; USD)	5,566,656	11,133,311	16,699,987	22,266,642	27,833,298
Plant decommissioning (USD)	3,885,987	7,771,974	11,657,976	15,543,963	19,429,951
Total actualized costs (USD)	123,528,723	24,7057,445	370,586,618	494,115,341	617,644,063

Based on the reported values, the costs are evenly distributed across all configurations. The largest contribution, CAPEX, represents 69% of the total plant cost. Actualized OPEX accounts for 24% (23% in an LBPV plant) of the total cost. Inverter replacement and plant decommissioning, at 4% (5% in an LBPV plant) and 3%, respectively, represent the smallest-cost items.

Figure 10 shows the total actualized cost of the three configurations for varying PV coverage ratios. As expected, the FPV_Track plant is the most expensive because of the presence of the tracking system. The least expensive is the LBPV one, because no tracking system is included and because of a smaller support system and mounting cost. The FPV_noTrack configuration shows an intermediate value for all simulated coverage ratios. However, when calculating the LCOE, it is important to also consider the productivity of the plant. In the case of FPV plants, especially in the FPV_Track configuration, productivity is higher due to the cooling effect of the water basin. Figure 11 shows that, with 15% coverage, FPV_Track has the lowest LCOE. This result is encouraging and confirms the significant potential of floating photovoltaic applications.

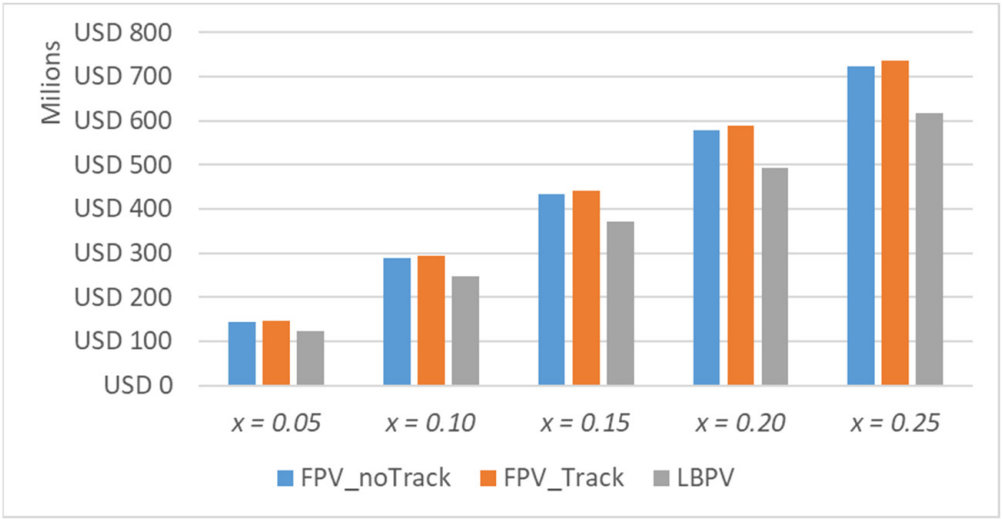

Figure 10. Total actualized cost of the three plants for different coverage ratios.

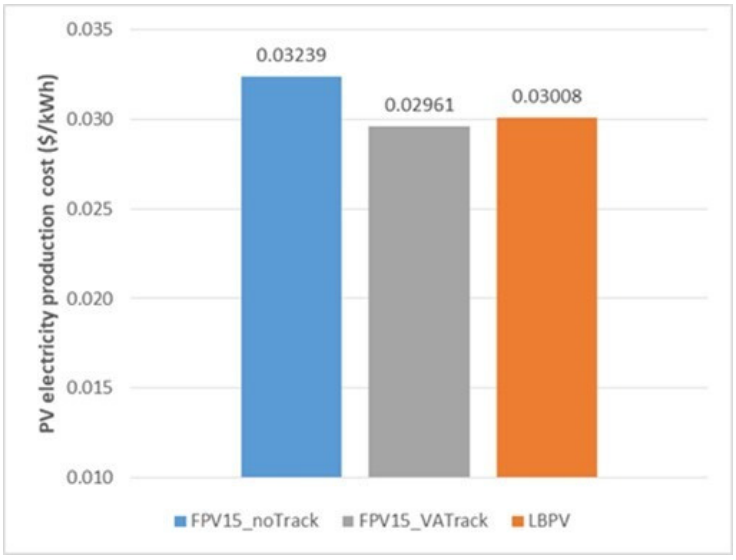

Figure 11. LCOE (USD/kWh) of the considered configurations, 15% basin coverage.

4. Conclusions

The present analysis examines the potential of implementing an FPV system in an Italian context, specifically focusing on the Cecita dam and Mucone I and II hydroelectric power plants located in southern Italy. The model presented and assessed in [14] is adopted to estimate the non-evaporated water in the case of FPV systems with varying coverage ratios (ranging between 5% and 25%). This allows for the calculation of the additional annual electricity production of the hydroelectric plants. Some main findings can be drawn from the analysis of the results:

- The larger the coverage ratio of the basin, the bigger the energy gain. In fact, with a coverage ratio of 25% the volume of water evaporated was about 5.31 Mm^3/y. This corresponds to an additional 10.154 GWh produced by the hydroelectric plant, which is 3.56% more than the reference case (i.e., no FPVs).
- The installation of a tracking system improves the production of a PV system for all the x values. The beneficial effect of the tracking system is noticeable even with a small coverage ratio. In fact, with only 5%, the annual energy production is comparable to that of the hydroelectric plant.
- Although the presence of the tracking system increased the total costs of FPV plants, they can still compete economically with common LBPV systems due to their higher productivity and the cooling effect of the water basin.

Coupling these results with possible benefits of FPVs, it becomes clear that this kind of application becomes very interesting to increase the renewable electricity production without requiring additional land use, which then can be dedicated to other applications. This, in turn, can help to reduce hydro turbine energy production during sunny periods, thus conserving the water reserve for water pumping or green hydrogen production.

Author Contributions: Conceptualization, P.V. and D.B.; methodology, P.V.; data curation, P.V.; writing—original draft preparation, P.V.; writing—review and editing, G.G.G., L.C., D.B., G.A. and M.V.M.C.; visualization, G.G.G. and G.A.; supervision, D.B., L.C. and P.V. All authors have read and agreed to the published version of the manuscript.

Funding: This research received no external funding.

Data Availability Statement: The data will be made available on reasonable request from the corresponding author.

Conflicts of Interest: The authors declare no conflicts of interest.

Nomenclature

AEW	annual evaporated water
BOS	balance of system
CAPEX	capital expenditure
E_{gain}	energy surplus
ER	evaporation rate
FPV	floating photovoltaic
FPV_noTrack	FPV, 15° tilt angle, no solar tracking (tested configuration)
FPV_Track	FPV, 15° tilt angle, vertical axis solar tracking (tested configuration)
g	gravity acceleration (m/s^2)
H_{mo}	average monthly sum of global irradiation per unit of surface (kWh/m^{2}mo)
h	water jump (m)
LBPV	land-based photovoltaic
NEW	non-evaporated water (mm/y)
NEWV	non-evaporated water volume (m^3/y)
OPEX	operational expenditure
PV	photovoltaic
RH	relative humidity (%)
R_S	daily horizontal solar radiation (MJ/m^{2}d)
S	surface (m)
T	mean daily temperature of air (°C)
t	time (s)
u_{10}	daily wind speed 10 m above the ground surface (m/s)
$\dot{V}$	volumetric flow rate (m^3/s)
VA	vertical axis
x	surface coverage ratio
Greek symbols	
α	tilt angle (°)
η	efficiency
ρ	density (kg/m^3)
Subscripts	
Free	open water
PVcover	water with FPV system
saved	non-evaporated
W	water

References

1. European Community. 'Fit for 55': Delivering the EU's 2030 Climate Target on the way to climate neutrality. In Proceedings of the Communication from the Commission to the European Parliament, the Council, the European Economic and Social Committee and the Committee of the Regions, Brussels, Belgium, 14 July 2021.
2. Energy Transition. Sectorial Strategic Guidelines. In *The 10 Fields of Actions of CDP 2022–2024 Strategic Plan*; CDP: Rome, Italy, 2021.
3. Ministry of Economic Development; Ministry of the Environment and Protection of Natural Resources and the Sea; Ministry of Infrastructure and Transport. *Integrated National Energy and Climate Plan*; European Commission: Rome, Italy, 2019.
4. Poongavanam, P.; Chand, A.A.; Tai, V.B.; Gupta, Y.M.; Kuppusamy, M.; Dhanraj, J.A.; Velmurugan, K.; Rajagopal, R.; Ramachandran, T.; Prasad, K.A.; et al. Annual Thermal Management of the Photovoltaic Module to Enhance Electrical Power and Efficiency Using Heat Batteries. *Energies* **2023**, *16*, 4049. [CrossRef]
5. Terna. *Renewable Evolution—2021 Development Plan*; Terna: Rome, Italy, 2021. (In Italian)
6. Dal Verme, M.; Lipari, D.; Lucido, G.; Maio, V.; Surace, V.; Liberatore, P. Statistical Report 2021. In *Energy from Renewable Sources in Italy*; GSE: Rome, Italy, 2023. (In Italian)
7. Ember Coal to Clean Energy Policy. In *Italy: Falling behind in the Electricity Transition*. 2022. Available online: https://ember-climate.org/app/uploads/2022/02/NECP-Factsheet-Italy.pdf (accessed on 27 January 2024).
8. Maghami, M.R.; Hizam, H.; Gomes, C.; Radzi, M.A.; Rezadad, M.I.; Hajighorbani, S. Power Loss Due to Soiling on Solar Panel: A Review. *Renew. Sustain. Energy Rev.* **2016**, *59*, 1307–1316. [CrossRef]
9. Victoria, M.; Haegel, N.; Peters, I.M.; Sinton, R.; Jäger-Waldau, A.; del Cañizo, C.; Breyer, C.; Stocks, M.; Blakers, A.; Kaizuka, I.; et al. Solar Photovoltaics Is Ready to Power a Sustainable Future. *Joule* **2021**, *5*, 1041–1056. [CrossRef]
10. Jäger-Waldau, A. *PV Status Report 2018*; EUR 29463 EN; Publications Office of the European Union: Luxembourg, 2018.
11. Cazzaniga, R.; Rosa-Clot, M. The Booming of Floating PV. *Sol. Energy* **2021**, *219*, 3–10. [CrossRef]

12. Ramachandran, T.; Mourad, A.-H.I.; Hamed, F. A Review on Solar Energy Utilization and Projects: Development in and around the UAE. *Energies* **2022**, *15*, 3754. [CrossRef]
13. Gorjian, S.; Sharon, H.; Ebadi, H.; Kant, K.; Scavo, F.B.; Tina, G.M. Recent Technical Advancements, Economics and Environmental Impacts of Floating Photovoltaic Solar Energy Conversion Systems. *J. Clean. Prod.* **2021**, *278*, 124285. [CrossRef]
14. Rosa-Clot, P. FPV and Environmental Compatibility. In *Floating PV Plants*; Elsevier: Amsterdam, The Netherlands, 2020; pp. 101–118.
15. Cazzaniga, R.; Cicu, M.; Rosa-Clot, M.; Rosa-Clot, P.; Tina, G.M.; Ventura, C. Floating Photovoltaic Plants: Performance Analysis and Design Solutions. *Renew. Sustain. Energy Rev.* **2018**, *81*, 1730–1741. [CrossRef]
16. World Bank Group; ESMAP; SERIS. *Where Sun Meets Water: Floating Solar Market Report*; World Bank: Washington, DC, USA, 2018.
17. Roesch, R. *Energy from the Sea: An Action Agenda for Deploying Offshore Renewables Worldwide*; International Renewable Energy Agency: Masdar City, United Arab Emirates, 2021.
18. SolarPower Europe. *Floating PV Best Practice Guidelines Version 1.0*; SolarPower Europe: Brussels, Belgium, 2023.
19. Polemio, M.; Casarano, D. Climate Change, Drought and Groundwater Availability in Southern Italy. *Geol. Soc. Lond. Spec. Publ.* **2008**, *288*, 39–51. [CrossRef]
20. Colangelo, M.; Camarero, J.J.; Borghetti, M.; Gentilesca, T.; Oliva, J.; Redondo, M.-A.; Ripullone, F. Drought and Phytophthora are Associated with the Decline of Oak Species in Southern Italy. *Front. Plant Sci.* **2018**, *9*, 1595. [CrossRef]
21. Spinoni, J.; Vogt, J.V.; Naumann, G.; Barbosa, P.; Dosio, A. Will Drought Events Become More Frequent and Severe in Europe? *Int. J. Climatol.* **2018**, *38*, 1718–1736. [CrossRef]
22. Ramasamy, V.; Margolis, R. *Floating Photovoltaic System Cost Benchmark: Q1 2021 Installations on Artificial Water Bodies*; National Renewable Energy Laboratory: Golden, CO, USA, 2021.
23. Silvério, N.M.; Barros, R.M.; Tiago Filho, G.L.; Redón-Santafé, M.; dos Santos, I.F.S.; de Mello Valerio, V.E. Use of Floating PV Plants for Coordinated Operation with Hydropower Plants: Case Study of the Hydroelectric Plants of the São Francisco River Basin. *Energy Convers. Manag.* **2018**, *171*, 339–349. [CrossRef]
24. Farrar, L.W.; Bahaj, A.B.S.; James, P.; Anwar, A.; Amdar, N. Floating Solar PV to Reduce Water Evaporation in Water Stressed Regions and Powering Water Pumping: Case Study Jordan. *Energy Convers. Manag.* **2022**, *260*, 115598. [CrossRef]
25. Trapani, K.; Redón Santafé, M. A Review of Floating Photovoltaic Installations: 2007–2013. *Prog. Photovolt. Res. Appl.* **2015**, *23*, 524–532. [CrossRef]
26. Tina, G.; Cazzaniga, R.; Rosa-Clot, M.; Rosa-Clot, P. Geographic and Technical Floating Photovoltaic Potential. *Therm. Sci.* **2018**, *22*, 831–841. [CrossRef]
27. Finch, J.W.; Hall, R.L. *; Environment Agency. Estimation of Open Water Evaporation: Guidance for Environment Agency Practitioners*; Environment Agency: Bristol, UK, 2001; ISBN 1857056035.
28. Finch, J.W.; Hall, R.L. *; Environment Agency. Estimation of Open Water Evaporation: A Review of Methods*; Environment Agency: Bristol, UK, 2001; ISBN 1857056043.
29. Penman, H.L. Evaporation in nature. *Rep. Prog. Phys.* **1948**, *11*, 366–388. [CrossRef]
30. Allen, R.G.; Pereira, L.S.; Raes, D.; Smith, M. *FAO Irrigation and Drainage Paper No. 56. Crop Evapotranspiration (Guidelines for Computing Crop Water Requirements)*; FAO: Rome, Italy, 1998.
31. Walter, I.A.; Allen, R.G.; Elliott, R.; Itenfisu, D.; Brown, P.; Jensen, M.E.; Mecham, B.; Howell, T.A.; Snyder, R.; Eching, S.; et al. *ASCE Standardized Reference Evapotranspiration Equation*; Environmental and Water Resources Institute of the American Society of Civil Engineers: Reston, VA, USA, 2021.
32. Bontempo Scavo, F.; Tina, G.M.; Gagliano, A.; Nižetić, S. An Assessment Study of Evaporation Rate Models on a Water Basin with Floating Photovoltaic Plants. *Int. J. Energy Res.* **2021**, *45*, 167–188. [CrossRef]
33. PVGIS Online Tool. Available online: https://re.jrc.ec.europa.eu/pvg_tools/en/tools.html (accessed on 10 January 2024).
34. Shuttleworth, W.J. *Known Typographic Errors in Terrestrial Hydrometeorology*; Wiley-Blackwell: Hoboken, NJ, USA, 2012.
35. Valiantzas, J.D. Simplified Versions for the Penman Evaporation Equation Using Routine Weather Data. *J. Hydrol.* **2006**, *331*, 690–702. [CrossRef]
36. Carl, R. *Evaporation from Free Water Surfaces*; Technical Bulletin; Western Michigan University: Kalamazoo, MI, USA, 1931.
37. Egré, D.; Milewski, J.C. The Diversity of Hydropower Projects. *Energy Policy* **2002**, *30*, 1225–1230. [CrossRef]
38. Gallo, L.; Battegazzore, M.; Corapi, A.; Lucadamo, L. Changes in Epilithic Diatom Communities and Periphytic Biomass Downstream of a Reservoir on a Mediterranean River (Calabria Region, S Italy). *Turk. J. Bot.* **2015**, *39*, 555–569. [CrossRef]
39. Direzione Generale per le Dighe e le Infrastrutture Idriche. Diga di Cecita (Cecita Dam). Available online: https://dgdighe.mit.gov.it/categoria/articolo/_dighe_di_rilievo/diga_di_cecita (accessed on 27 April 2023). (In Italian)
40. S.M.E.—Società Meridionale di Elettricità. *Impianti Idroelettrici sul Fiume Mucone*; S.M.E.—Società Meridionale di Elettricità: Napoli, Italy. (In Italian)
41. Abdelgaied, M.; Kabeel, A.E.; Zeleňáková, M.; Abd-Elhamid, H.F. Floating Photovoltaic Plants as an Effective Option to Reduce Water Evaporation in Water-Stressed Regions and Produce Electricity: A Case Study of Lake Nasser, Egypt. *Water* **2023**, *15*, 635. [CrossRef]
42. DXM8-66H/BF 490-505W M8 Steel Series, Sun-Earth Italia. Available online: https://sun-earth.it/prodotti/moduli-dxm-dxp/ (accessed on 27 April 2023).

43. Cazzaniga, R.; Rosa-Clot, M.; Rosa-Clot, P.; Tina, G.M. Integration of PV Floating with Hydroelectric Power Plants. *Heliyon* **2019**, *5*, e01918. [CrossRef] [PubMed]
44. Grubišić-Čabo, F.; Nižetić, S.; Marco, T.G. Photovoltaic panels: A review of the cooling techniques. *Trans. FAMENA* **2016**, *40*, 63–74.
45. Goswami, A.; Sadhu, P.; Goswami, U.; Sadhu, P.K. Floating Solar Power Plant for Sustainable Development: A Techno-Economic Analysis. *Environ. Prog. Sustain. Energy* **2019**, *38*, e13268. [CrossRef]
46. Rosa-Clot, M.; Tina, G.M.; Nizetic, S. Floating Photovoltaic Plants and Wastewater Basins: An Australian Project. In *Proceedings of the Energy Procedia*; Elsevier: Amsterdam, The Netherlands, 2017; Volume 134, pp. 664–674.